CHARACTERISTICS OF DYNAMICALLY FORMED OXIDE FILMS IN Al–Zn MELT

**Nader Taheri Bagh, Mehdi Divandari (iD), Mohammad Shahmiri, and Mehdi Akbarifar**
School of Metallurgy and Materials Engineering, Iran University of Science and Technology (IUST), Narmak, Tehran 16846-13114, Iran

Abstract *The entrainment of surface oxide films in the melt leads to the formation of double oxide defects in the casting parts. Oxide/metal/oxide (OMO) sandwich technique is a method for physical simulation of the formation of surface oxide film. In this method, air bubbles are artificially introduced into the melt in order to trap two adjacent bubbles and extract the interface between them. In this study, to prepare OMO samples, air bubbles were blown with a pressure of 0.8 atm. into the mold filled with Al melt containing 3, 5 and 7 wt% of Zn. Using scanning electron microscopy and energy-dispersive X-ray spectroscopy, characteristics of dynamically formed oxide films such as morphology and film thickness were investigated. Results showed that in higher zinc content, more cracks appear on the oxide films. Thickness of the oxide films in Al–Zn alloys was estimated to be 95–1070 nm. According to the measurement performed on the folds, adding more than 3% zinc caused a reduction in the oxide film thickness. Thermodynamics suggests the presence of spinel phase along with aluminum oxide at 700 °C which is in agreement with energy-dispersive X-ray spectroscopy's results. The presence of the spinel phase at the interface is the reason behind the reduction in the thickness of the oxide film.*

Graphic Abstract
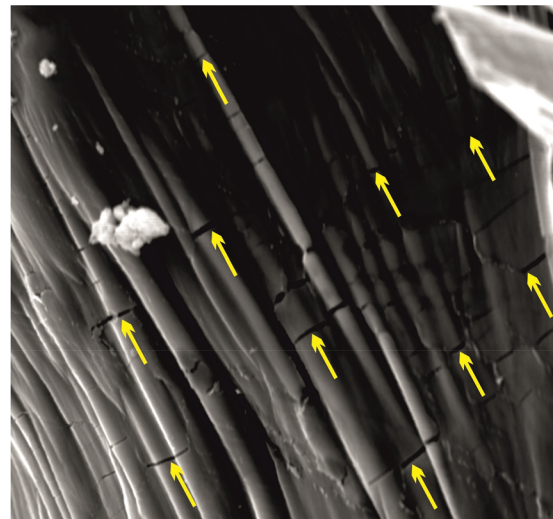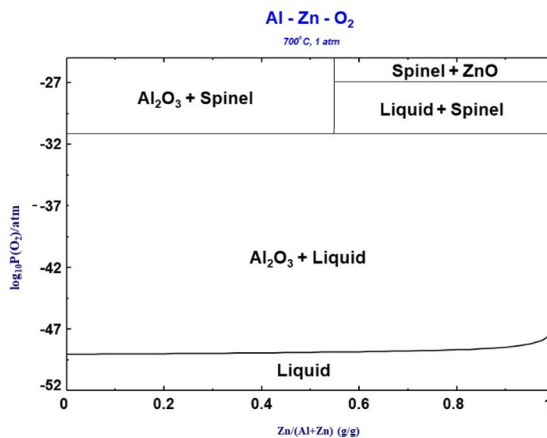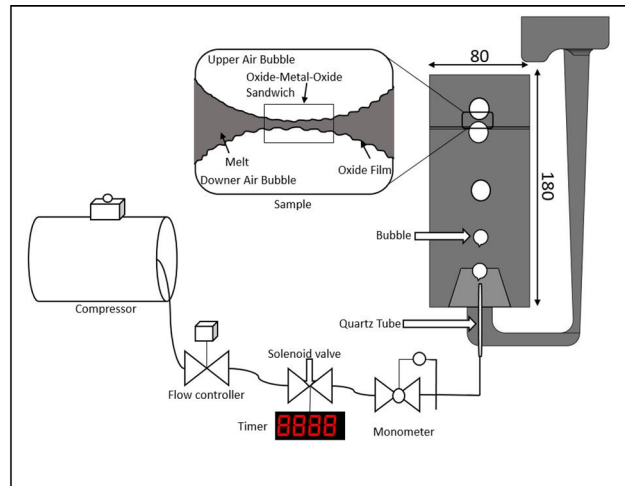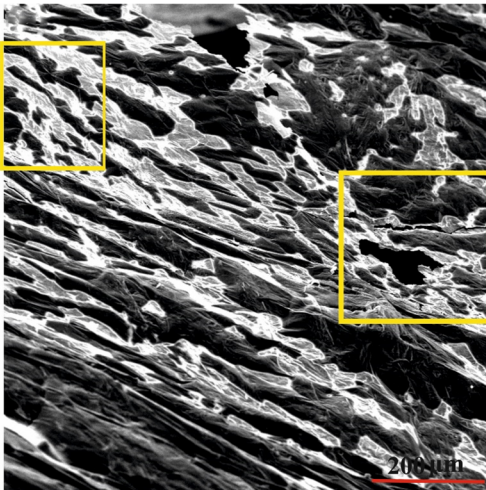
Introduction

Aluminum alloys show a high affinity to react with oxygen, oxidizing with a high rate in the molten state. Several parameters including temperature, alloying elements, humidity and testing procedure govern the oxidizing reaction, especially nucleation and growth stage of oxide layers.[1] The effect of addition of 1 at.% of various alloying elements at 700 and 800 °C on the oxidation behavior of Al melt is investigated. It is expressed that Zn has no noticeable effect on the oxidation process at 700 °C, but at 800 °C, the effect is pronounced.[2]

Exposing molten Al to air, an amorphous layer of γ-Al_2O_3 will appear on the surface.[3,4] Following that, crystalline particles of γ-Al_2O_3 will nucleate on the oxide/metal interface. With the further growth of these particles, a continuous layer is formed. The transition of γ-Al_2O_3 to α-Al_2O_3 is expected after an incubation period. Consequently, due to the smaller unit cell volume of α-Al_2O_3, the number of cracks on the oxide layer can increase. This results in the less protection of the metal in comparison

with that of γ-Al_2O_3.[5,6] Oxidation in the molten stage can be categorized into the static and dynamic modes. Wightman and Frei reported that the oxidization in the dynamic mode would be about 60 times faster compared to the static mode.[7]

The surface oxide layer on the molten metal experiences turbulence during the transformation from the furnace to the mold and especially within the pouring stage. This leads to the further break and rupture of the oxide layer. Consequently, the bare metal will be immediately exposed to atmosphere and a new oxide layer will form.[8–10] The frequent formation and rupture of oxide layers which occur in turbulent situations are called dynamic oxidation. Although many published results reported on the static oxidation of the molten metal, in the last few years dynamic oxidation became center of scientific and industrial attention on the arrival of the controversial theory of bifilms.[8]

Surface oxide film is dragged and trapped within the liquid as a result of melt turbulence.[7–9] Bifilms are combined of two oxide layers wrapped on each other, unwetted sides of the films coming together, face to face, so that little or no bonding occurs between the two. The double oxide feature acts as a crack in the liquid. The absence of any bonding between the two layers leads to their high potential to act as nucleation sites for gas porosities and shrinkage cavities.[7,11–13]

The mechanical properties and the reliability of cast aluminum alloys are closely related to their concentration of bifilms. This damage is maximized in case of the bifilms being unraveled and flattened.[8] Clearly, the elimination of these defects would lead to the production of casting parts with higher mechanical properties and reliability.[14–16]

A method to investigate the oxidation of molten metal during the pouring stage of castings is introduced based on the controlled introduction of bubbles into the melt.[17,18] In this method, the interface between two trapped bubbles provides an oxide/metal/oxide (OMO) sandwich which yields information about the morphology, thickness, chemical composition and strength of oxide films. The melt trapped between the oxide films of two air bubbles appears as a thin layer, in the range of 10 μm or so, but normally

thick enough that some nuclei start dendritic solidification. This thin layer of the sample, known as OMO sandwich, can show some details of the important stage of solidifying of the melt and the features of oxide film.[19–21] The optimum conditions to produce an OMO sandwich have been previously reported by the authors.[17–21]

Characteristics of oxide films are strongly related to the composition. Haginoya et al. have investigated the effect of Zn addition on the oxidation of aluminum melt at various temperatures.[22] Zinc causes a reduction in the oxidation rate of aluminum rate below 700 °C but acts conversely at temperatures above 800 °C. Furthermore, Zn extends the incubation time for the transformation of the amorphous alumina to the crystalline γ-alumina, a transition which would normally be accompanied by the formation of cracks on the oxide film. Apart from that, Zn enters the crystalline structure of γ-alumina and reduces the number of cation vacancies. Consequently, less aluminum cations would be able to reach the other side of the film to interact with oxygen ions. Therefore, the slope for the oxidation diagram of aluminum–zinc alloy would decrease with time. The boiling point of the zinc would be a problem at higher temperatures. In that case, the formation of zinc oxide and $ZnAl_2O_4$ spinel would be expected.[22] The lattice parameter of $ZnAl_2O_4$ is bigger than alumina's, and this would cause local stresses in favor of accelerating the oxidation process.

The strength of the oxide layer also matters. Oxides with higher strength would be more resistant to cracks.[23] Apart from that, structure, morphology and thickness of these layers would play a crucial role in the quality of casting parts.

Studies have shown that 1 wt% of the total aluminum melt will be oxidized during casting process.[1] Therefore, considering the effect of the bifilm defect on the mechanical properties of the product and its quality index,[8,15] understanding the nature and characteristics of the formed oxide films is crucial. Addition of elements and impurities affects the oxidation rate and characteristics of the oxide film. Accordingly, the effect of addition of elements such as magnesium, calcium and strontium on dynamically formed oxide films in aluminum alloys has been investigated.[5,8,9,11,19] But to the authors' knowledge, effect of Zn addition and its consequent effect on the thermodynamics of oxidation in the aforementioned dynamic situation are still neglected in the literature.

In the present study, the effect of Zn content on the characteristics of dynamically formed oxides of aluminum alloy has been studied via oxide/metal/oxide sandwich method. Thickness of oxide films along with the morphological features was investigated by scanning electron microscopy equipped with energy-dispersive X-ray spectroscopy.

Table 1. Chemical Composition of Samples Per wt% (Rounded)

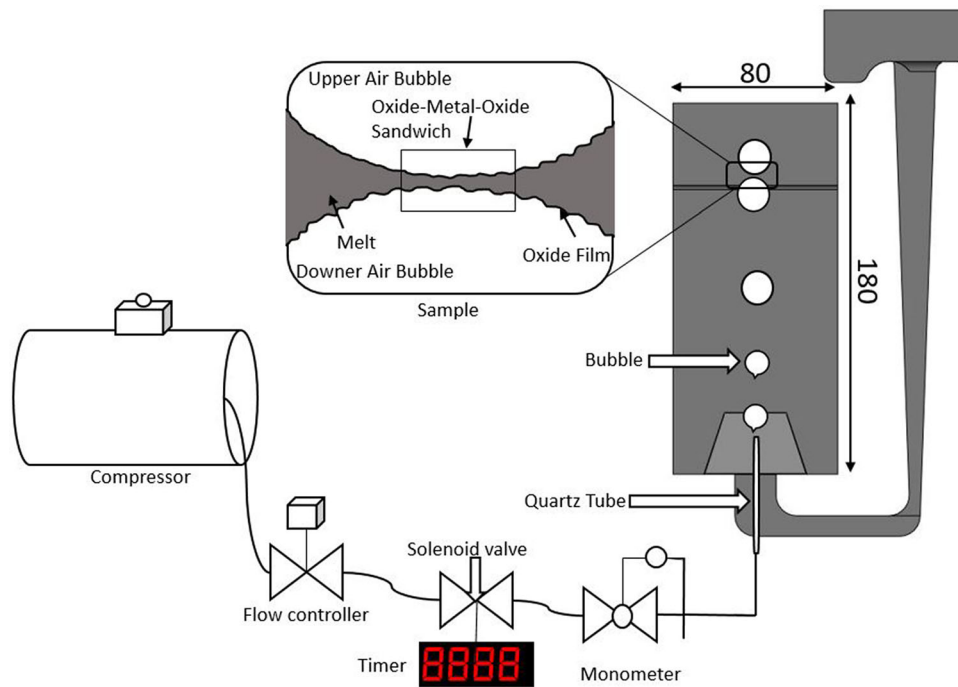| Alloy	Element			
	Al%	Zn%	Cu%	Fe%
Al–3%Zn	96.2	3.1	0.3	0.2
Al–5%Zn	93.5	5.7	0.3	0.25
Al–7%Zn	92.1	7.2	0.24	0.2

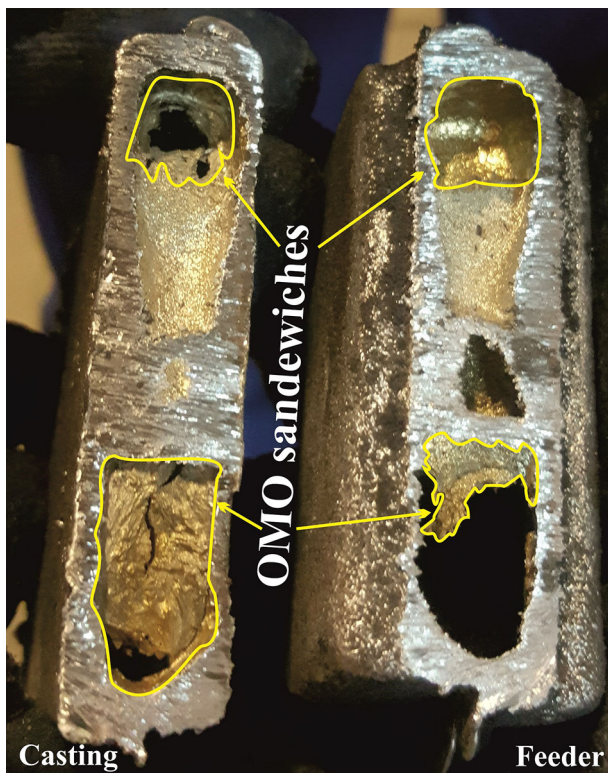*Figure 1. Schematic of the bubble blowing procedure and mold used in the present study.*

Figure 2. Oxide–metal–oxide sandwich samples within the cast metal.

Materials and Methods

The casting model was designed based on the criteria for the bottom gated running system.[8] The model has gone through computational fluid dynamic (CFD) simulations in order to evaluate mold cavity filling, solidification process and flow rate of molten metal entering the mold cavity which is reported elsewhere.[21]

To prepare the melt, commercially pure aluminum and Al–Zn 20 wt% master alloy was used. Pouring temperature was chosen 30 °C above the liquidus temperature of each alloy according to the phase diagram. A clay graphite crucible was employed to hold the melt in a resistance furnace. All the tools, e.g., crucible, mold, etc., used in the casting process were preheated up to 100 °C. The final composition of each sample according to spectral analyzers results is given in Table 1. These are the average numbers acquired from an optical emission spectrometer performed on the samples cut from the cast.

After reaching the appropriate composition, molten metal was poured into the sodium silicate–sand mold. To generate artificial bubbles in a certain shape and size and blowing them at the predefined time intervals of two bubbles per second, a system was designed.[9,21] In this
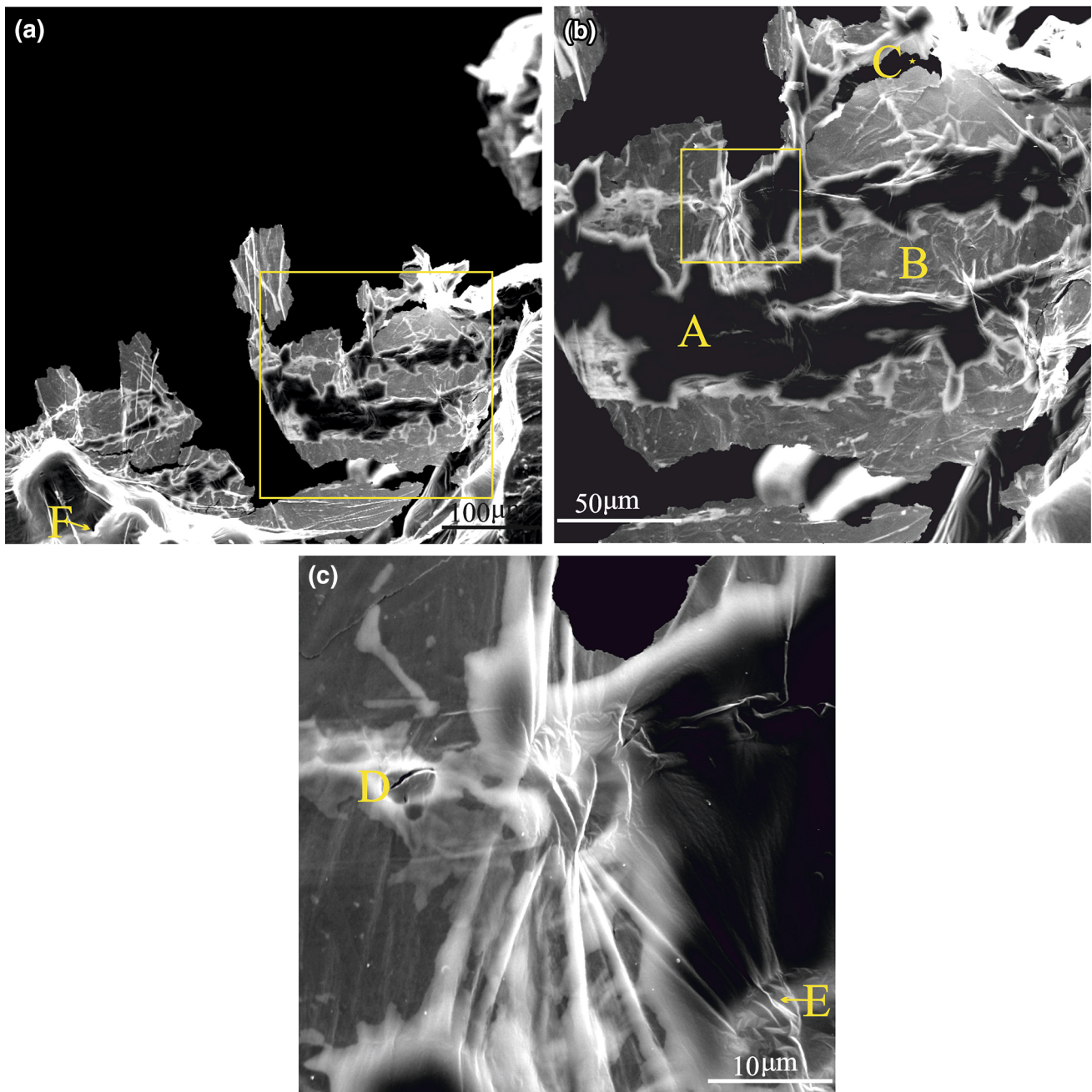
Figure 3. *Secondary electron (SE) micrographs of OMO sandwich formed in Al–7% Zn alloy. The images are magnified in order (a–c). Represented regions are the entrapped metal between two oxide layers (A), two adjacent oxide layers (B), large cracks (C), cracks formed due to the stresses during solidification process (D), wrinkles caused by the difference in the thermal expansion coefficient of metal and oxide (E) and the cavities made by the impression of dendrite growth on the surface oxide covering it (F).*

setup, the compressor produces the compressed air and its pressure reaches the specific value passing through a few instruments including solenoid and control valves. The setup used to introduce bubbles into the melt is presented in Figure 1. A quartz tube with inner diameter of 1 mm was placed in the bottom of the mold. Bubbles were blown with a pressure of 0.8 atm. Proper pressure depends on the density of liquid metal and the head of molten metal in the mold.[16,19]
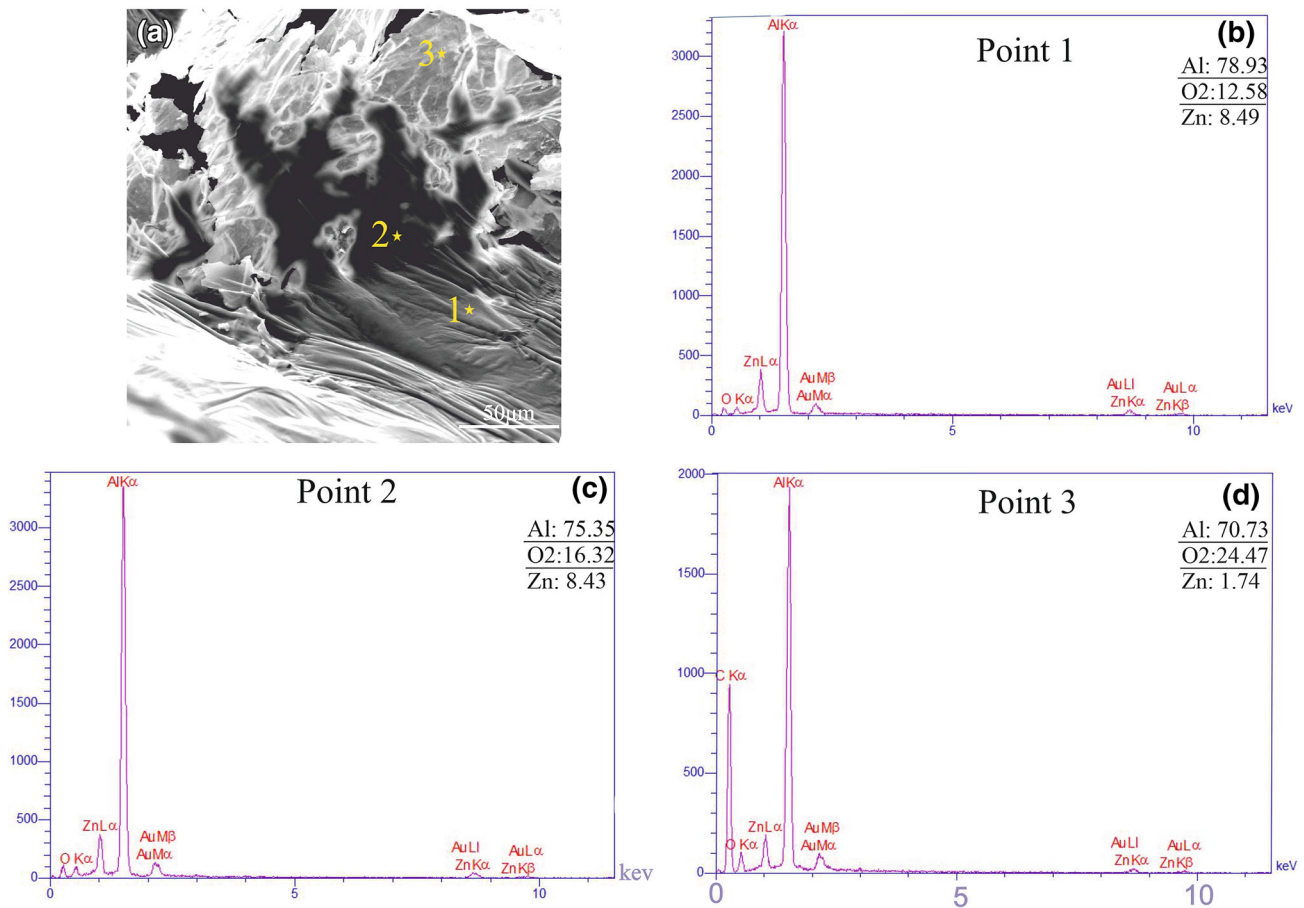
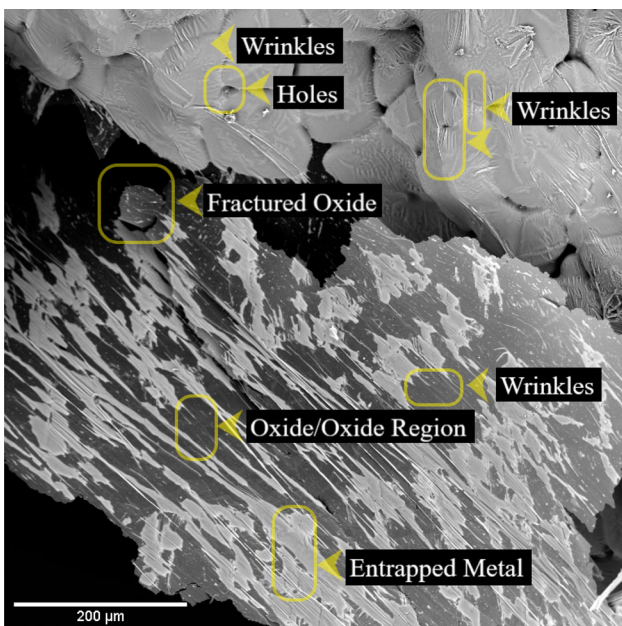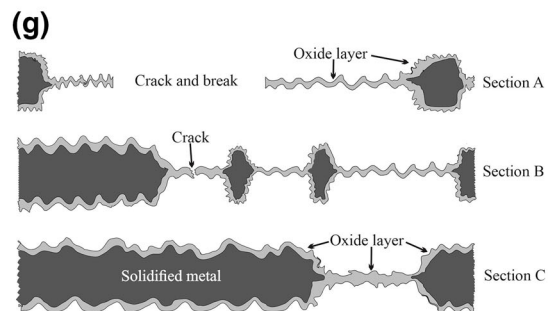**Figure 4. SEM image from the surface of Al–5%Zn OMO sandwich and EDS analysis from points 1, 2 and 3.**

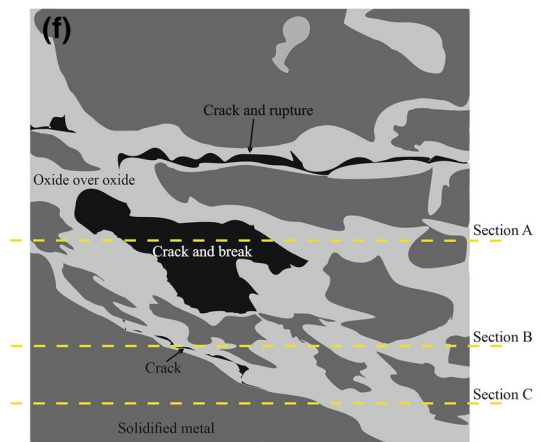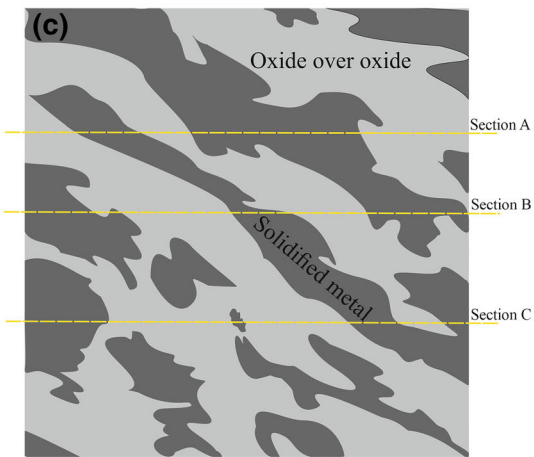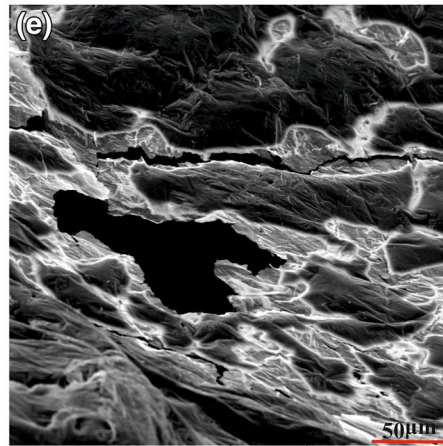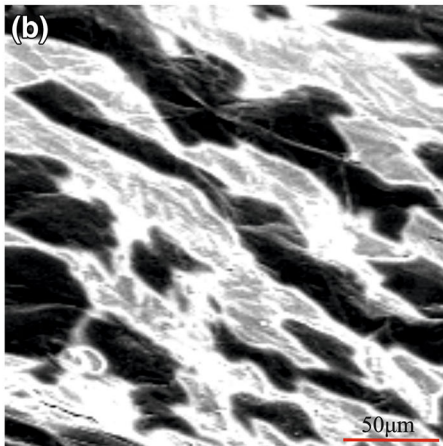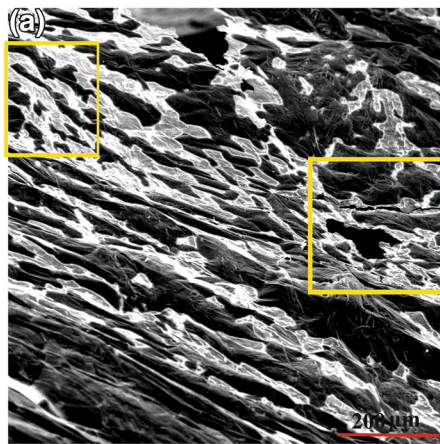**Figure 5. Backscattered electron (BSE) micrograph of Al–7%Zn OMO, providing better resolution of the folds and wrinkles formed on the sandwich sample. It also shows areas containing trapped metal between oxide layers, double oxide layers and interdental cavities.**

The model used in this study includes a plate pattern with dimensions of 180×80 mm and a thickness of 20 mm. On top of the model, a top feeder is added to increase the chances of air bubbles getting trapped. At the bottom of the model, two trapezium-shape feeders are used to create a warm region around the tip of the quartz tube. With this operation, until the last stage of solidification, there is a chance to insert artificial bubbles. The mold used, silica sand, contains 4% of sodium silicate as the binder.

Schematic of oxide/metal/oxide sandwich production is illustrated in Figure 1. When the pouring step was done, artificial bubbles were released with specified time intervals (two bubbles per second). After successfully performing the procedure, the final cast was cooled in the air and cut in pieces.

Figure 2 shows the sandwiches before being cut off from the casing. After cutting off, the OMO sandwiches were gold-coated by ion sputtering. Eventually, the samples were investigated by scanning electron microscopy (SEM), Vega 2 TESCAN, equipped with energy-dispersive spectroscopy (EDS). Also, the phase diagrams of Al–Zn–O system were calculated using FactSage 7.3.

(a)

(b)   (e)

(c)   (f)

Oxide over oxide   Crack and rupture

Section A   Oxide over oxide

Section B   Crack and break   Section A

Solidified metal   Section B

Section C   Crack   Section C

                                       Solidified metal

(d)   (g)

Oxide layer   Oxide layer
Solidified metal   Section A   Crack and break   Section A

Oxide layer   Crack
Solidified
metal   Section B   Section B

Oxide layer
Solidified metal   Section C   Solidified metal   Oxide layer   Section C

Figure 6. SEM image and its schematic of Al–7%Zn OMO sandwich in secondary electron mode that show (a) SEM image of Al–7%Zn OMO sandwich, (b) the magnified image of the rectangular area marked in upper left of image (a), (c) schematic of the image (b) explaining the detail, (d) schematic of the cross sections in three positions—A, B and C—for clarification, (e) the magnified image of the area marked in the right-middle part of the main image, (f) schematic of the image (e) showing other features of OMO sandwich, (g) cross sections of three lines—A, B and C—in the image (f).

Results and Discussion

Morphology

SEM images of oxide/metal/oxide sandwich of Al–7%Zn alloy showing typical features are shown in Figure 3. Features include the entrapped metal between two oxide layers (A), two adjacent oxide layers (B), large cracks formed during extraction of sandwiches (C), cracks formed due to the stresses caused from the solidification shrinkage and mechanical stresses (D), wrinkles caused by the difference in the thermal expansion coefficient of metal and oxide (e) and the cavities made by the impression of dendrite growth on the surface oxide covering it (F).

SEM image of OMO sandwich from Al–5%Zn sample is demonstrated in Figure 4. EDS analysis results prove the appearance of oxide phase.

Folds and wrinkles are clearly visible on the surface of the oxide layer in Figure 6. In contrast to other images shown in this work, which are mostly secondary electron micrographs, Figure 5 shows a backscattered micrograph giving a better idea of the characteristics of the OMO sandwich.

The oxide film and aluminum melt are, of course, in intimate atomic contact (the oxide having grown atom by atom from the metal surface).[24,25] Therefore, the oxide films necessarily follow the turbulence in the melt, folding and tearing in the chaotic flow of the melt, particularly during the pouring and the filling stages. In such conditions, if the surface oxide on the melt is torn, a new oxide layer would form on the newly exposed surface. If the surface is folded, the basic mechanics of surface behavior are complicated:

The folds entrap air between the upper dry sides of surface films but entrap metal between the wetted undersides of films. Further shrinkage of the surrounding metal during the solidification would cause deformations on the film surface which is known as wrinkles.

Apart from that, the solidification of entrapped melt between the oxides would cause deformations through suction of the thin layers of entrapped liquid metal and drawing them inward.

Returning to the detail of OMO formation, which is a collision between the wetted sides of two oxide films of two consecutive bubbles, the molten metal may be partially driven outward by the lower bubble buoyancy force. Figure 6 shows an arrangement of SEM images and their graphical views of the sandwich formed between two adjacent bubbles in Al–7%Zn alloy, including two selected areas: the first one (Figure 6b) chosen from the upper-left part of the image and the second (Figure 6e) from the middle-right part and their cross sections in different positions (Figure 6d and g). Figure 6b shows a magnified portion of the sandwich sample containing overlapping oxide layers and metal between layers. No cracks are visible in the oxide films. Figure 7c shows the graphical view of Figure 6b in which islands of solidified melt are surrounded by overlapped oxide film. Three cross sections shown in Figure 6d depict the features of the OMO sandwich noting how the oxide layers from both sides capture the melt in between.

Figure 6e shows the second magnified part of the main image (Figure 6a). Figure 6f shows a schematic view of Figure 6e, depicting all the details of this figure. In this image, cracks are visible in black. OMO sandwich has torn in these locations due to the mechanical stresses caused by the dynamical motion of the bubbles in the melt. Moreover, stresses caused during extraction of the sample can be another source.[17–20] As mentioned above, the gray areas represent the overlying oxides and the black-tinted areas show the lost metal between the two oxide layers. The side view of the oxide/metal/oxide sandwich sample is shown in Figure 6g in three sections A, B and C.

General steps of OMO sandwich formation are illustrated in Figure 7. As can be seen, in the first stage (Figure 7a), it
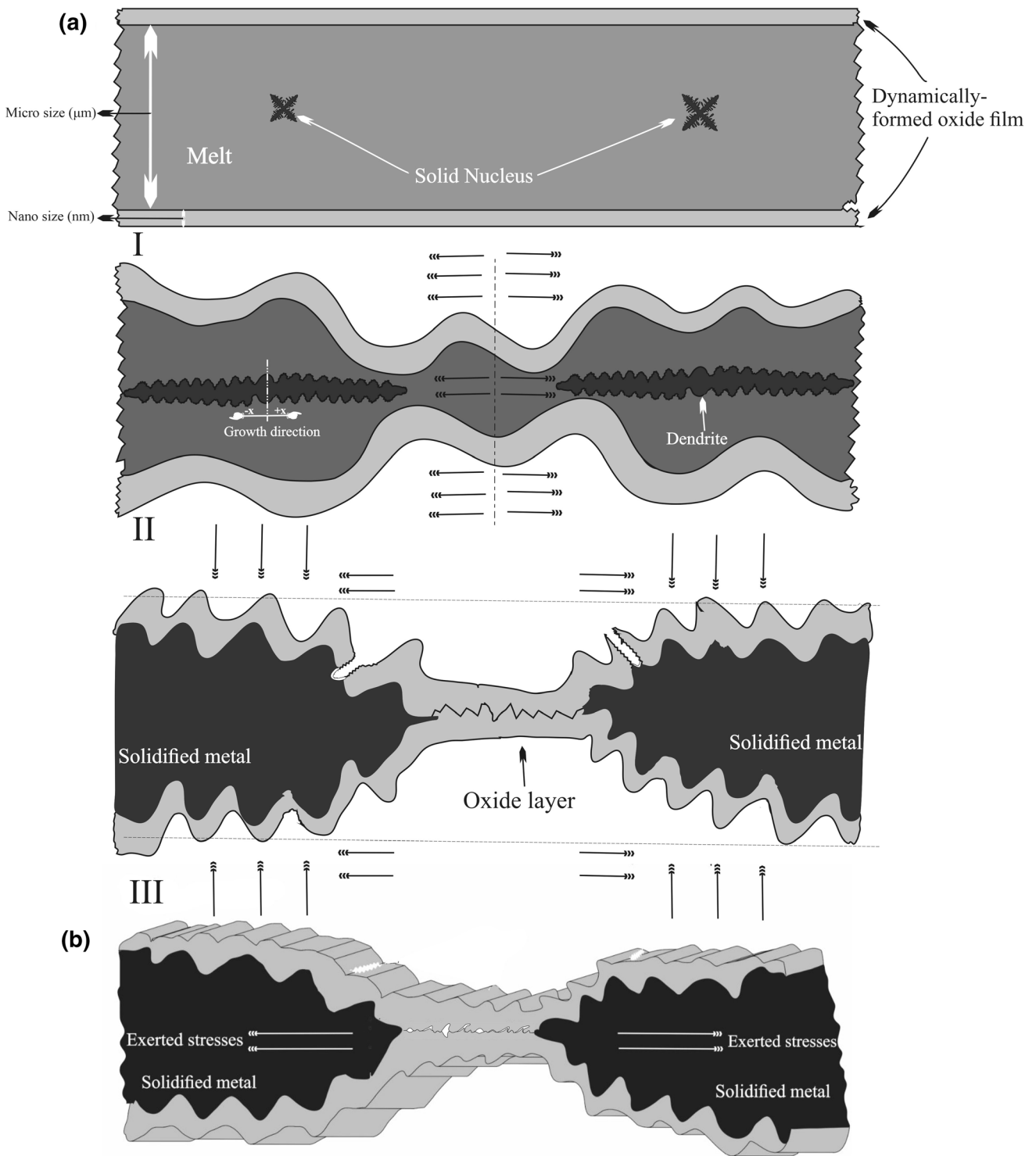
Figure 7. *(a) Schematic cross section of the OMO sandwich showing stages of solidification and possible events. Step I: Appearing of the solid nucleus within the melt in sandwich, step II: induced stresses in the metal due to melt suction and contraction pressure created during solidification process and step III: exerted stresses on the oxide film that lead to tearing, breaking and wrinkle forming on the oxide layer and (b) 3D schematic of the image (a—III).*
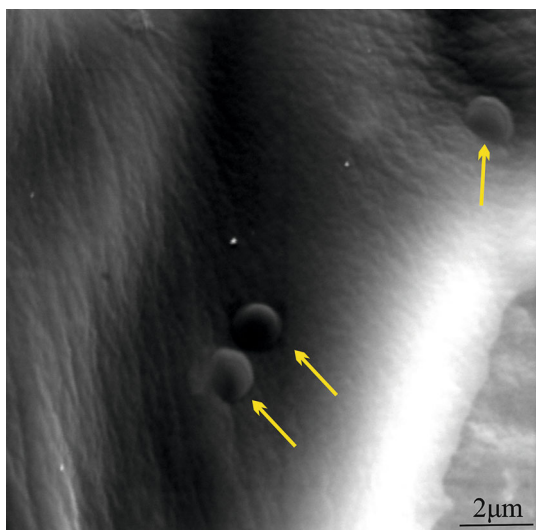
Figure 8. The presence of swells on the oxide film formed in Al–7%Zn alloy that indicated by arrows.

is imagined that some freezing nuclei may appear on the suitable place in the melt. It should be noted that while the melt is shrinking in several directions, the oxide film does not shrink in proportion to the melt. Although the molten metal has wettability with its surrounding oxide film, it does not fit the volume and longitudinal shrinkage coefficient of the oxide. So, folds would appear on the surface of oxide films to compensate the difference. At the same time, the surface oxide film starts to be sucked into the dendrite mesh which is forming. This is shown in stage 2 of Figure 7a. In the next stage, by completing the freezing, the tensile stress of the shrinkage force reaches its final level, causing the oxide film to crack in different places. The fact that the oxide film contains melt inclusions can explain the chance of cracking due to the presence of contraction stresses. Figure 8b shows the three-dimensional slice of the OMO sandwich.

Swell Formation

Having a closer look at the surface of the oxide film, some swells are observable (Figure 8). One possible cause is hydrogen, and another possible source is zinc vapor. The partial vapor pressure of different elements at 680 °C is given in Table 2. The high value of the Zn vapor pressure

Table 2. Partial Vapor Pressure and Boiling Point of Al and Zn[25]

Element	Temperature (°C)	Vapor pressure (atm.)	Boiling point (°C)
Al	680	7.97×10^{-12}	2519
Zn	680	4.16×10^{2}	907

indicates the zinc is probably a significant contributor to the blister formation, despite its reduced activity as a result of its dilution in the alloy. As in all varieties of pore formation, pressure due to both hydrogen and zinc could combine to create the defect.

The presence of such blisters on the oxide films of pure magnesium metal has been reported and linked to three different mechanisms: rejection of hydrogen atoms, vaporization of magnesium atoms and intrinsic defect of the oxide film.[26] As for the magnesium, Zn poses a high vapor pressure, too. Accordingly, in the case of Al–Zn alloy, evaporation of zinc atoms is more likely to be the mechanism behind the formation of blisters.

Oxide Film Thickness Estimation

The thickness of folds is affected by a various number of parameters such as the amount of material trapped within the fold, intensity of regional stresses in each fold, strength, and flexibility of oxide film, the tendency of the alloy to oxidation and also the amount of available oxygen in the vicinity.[7] In oxide film thickness estimation, the thinnest folds are assumed to have a low probability of entrapped material and so represent a doubling of the thickness of the film. Regions like point *B* in Figure 4 are the suitable places to search for a fold without any entrapped metal between two layers. Nevertheless, if the length or height of a fold is less than its width, the estimation could be accompanied by some error because of the possibility of some metal entrapment between the films. Figure 9 shows the schematics of morphological features of the oxide films which were used to estimate their thickness. Thickness would be equal to the measured value divided by two. Clearly, performing the measurements on the edge of the oxide film would result in a more precise value (Figure 9d). Figure 10 shows images of the OMO sandwiches used for thickness estimations in oxide films of samples with 3 and 7 wt% of Zn. Results are presented in Figure 11 as a diagram. Accordingly, the thickness of the formed oxide in Al–3%Zn alloy is within the range of 100–1000 nm.

Scattering in the thickness values of the oxide films indicates the complex procedure of the oxidation in dynamic situation. Entrapment of oxide films in the melt occurs quickly due to surface turbulence. So, these entrapped oxides had a little time to grow thick and become in the order of a few hundred of nanometers.[24]

Oxide Structure

Alumina exists with different atomic structures according to the formation temperature and elapsed time. Initially formed alumina at 750 °C is amorphous, with its growth controlled by the outward diffusion of aluminum cations.
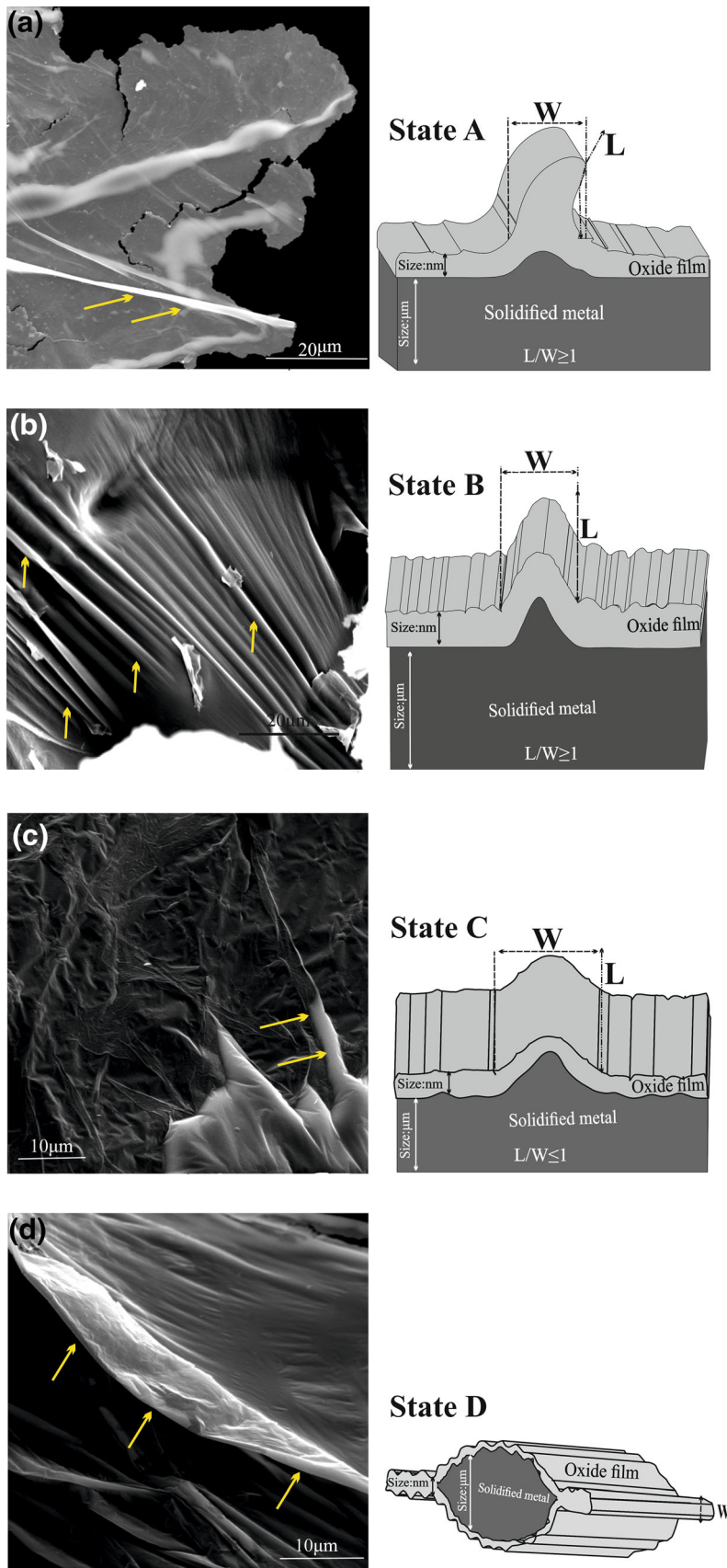
At high temperature, the amorphous growth is arrested by the nucleation and growth of crystalline γ-alumina. The controlling mechanism for growth of this phase is inward diffusion of oxygen anions. Alloying elements could affect the number of cationic or anionic vacancies in the oxide structure and, hence, make a change in the oxidation rate.[3] Most oxide structures consist of a compact network of oxygen anions with cations placed at octahedral or tetrahedral interstitial positions. Since only one-quarter of these positions would be occupied, cation diffusion is plausible even in the absence of vacancies. So, an intermittent chain of octahedral and tetrahedral vacancies would be an easy path for cation diffusion through the oxide layer.[27,28] Reported investigation has shown that the amorphous oxide structure has a stoichiometric ratio of $Al_{2-x}O_3$ with an approximate value of 0.42 for x; accordingly, oxygen is in excess in the structure and consequent growth of the oxide layer would be favorable.[29]

While according to Figure 1 addition of Zn to the aluminum melt should not affect the oxidation, the results of this investigation show a small reduction in the thickness of oxide films (Figure 11). It has been reported in the literature that introducing Zn to the aluminum leads to the formation of a relatively thin zinc oxide beneath the oxide layer, along with the incorporation of Zn ions in the amorphous alumina.[30] This thin zinc oxide layer would act as a barrier preventing the flow of aluminum cations. Then, the incubation time before the oxide rupture would be increased. The deficiency of vacancies and the dwindling mobility of oxygen anions through the oxide layer would control the reduction in the oxidation rate and therefore the oxide thickness.[4,31] In the case of gamma alumina, Zn would penetrate into the crystalline structure and decrease the number of interstitial positions. But such an explanation would be more appropriate for the case of long-term oxidation. In case of dynamically formed short-time oxides, referring to the PO_2 phase diagrams would be more reasonable.

Figure 12 shows the phase diagram plotted for Zn mass fraction versus oxygen partial pressure in Al–Zn system at 700 °C calculated by FactSage 7.3.[32] As it can be seen, oxidation of Al–Zn alloys at Zn contents within this study begins with the formation of Al_2O_3 at a very low oxygen pressure of 10^{-49} atm. It is only at the PO_2 of 10^{-31} atm. that formation of the spinel oxide would be possible. Therefore, the major part of the formed oxide layer would be composed of primary Al_2O_3, accompanied with spinel oxide. The only difference between the case for Al–Zn–O system and Al–O system would be the presence of the spinel phase. It seems spinel formation may be responsible for the decrease in the thickness of the oxide film with the addition of Zn to aluminum melt.

Hypothetically, flexibility of the oxide film has a remarkable effect on the oxidation rate.[26,33,34] In the case of low flexibility of oxide film, the surface film would be repetitively fractured due to the mechanical stresses caused by turbulence and shrinkage. This would lead to over and over exposure of the metal to the atmosphere and formation of new oxide layers. Consequently, the oxidation rate will be intensified.

Figure 13 shows the SEM images of the oxide films extracted from pure aluminum and Al–Zn alloys. The film observed in pure aluminum has been deformed and bent under the applied stress without any fractures. On the other hand, films from the Al–Zn alloys samples possess more cracks and torn regions. Supposedly, the presence of Zn reduces the flexibility of the film and leads to additional cracking behavior.[35]
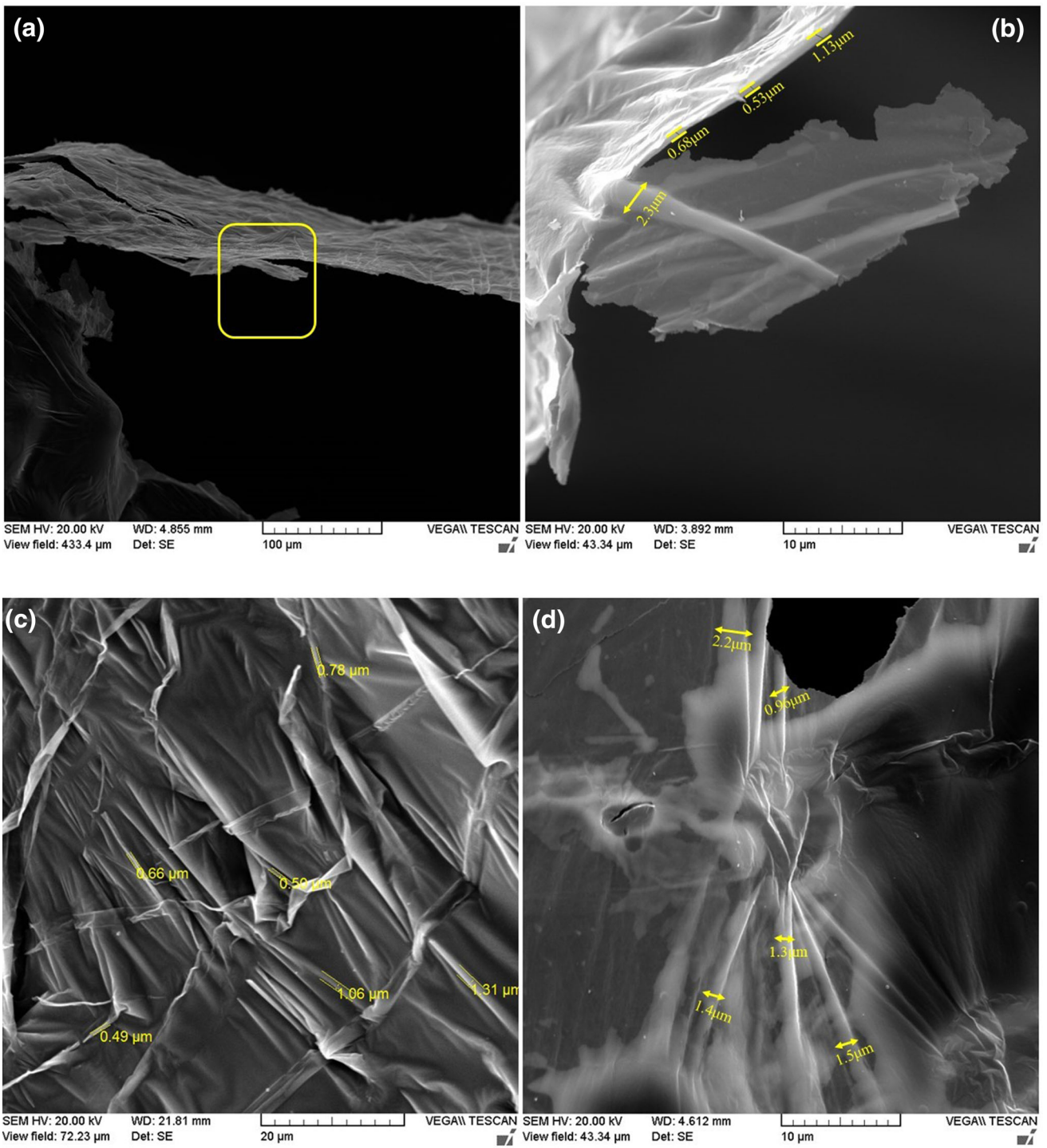
Figure 10. *Estimation of the oxide thickness by measuring the width of the folds and the edge layer in SEM images from different areas of OMO sandwich: (a) Al–7% Zn, (b) the magnified images of the marked area in images (a), (c) Al–3% Zn and (d) Al–7% Zn.*
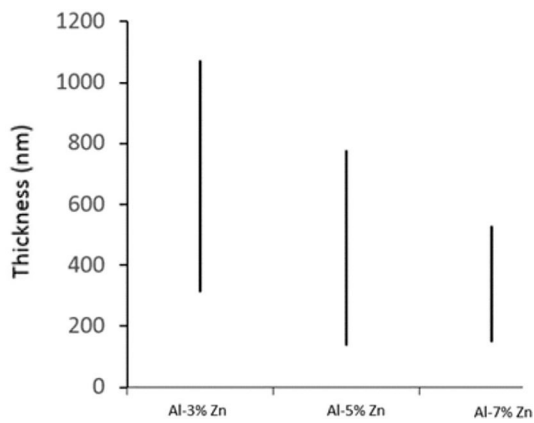
Figure 11. Results of thickness estimation of the oxide layer by measuring the width of the edge layer and fold in SEM images of Al–Zn alloys OMO sandwich.

Conclusion

In the present study, the oxide films formed on the Al–Zn alloys melt in dynamic conditions were investigated using oxide/metal/oxide (OMO) method. The following results were concluded:

1. Reduction in the thickness of oxide film by increasing the Zn content can be related to the presence of spinel phase.
2. Addition of Zn to aluminum melt leads to embrittlement of the oxide layer, reducing its flexibility and increasing the number of cracks.
3. The morphology of formed oxide film includes fold, wrinkle, crack, tear, hole and swell. Folds and wrinkles are the results of mechanical stresses caused by turbulence of the melt and shrinkage stresses during solidification. Holes and swells seem to be related to solidification stage.
4. The cause for the formation of swells on oxide surface is yet unknown. Among the proposed mechanisms, evaporation of Zn atoms is more likely to be the reason.
5. The range of the thickness value of the dynamically formed oxides of Al–Zn system was reduced by addition of more Zn. Thickness range in Al–3%Zn alloy varies between 100 and 1000 nm, but in Al–7%Zn alloy, the maximum value is about 600 nm.
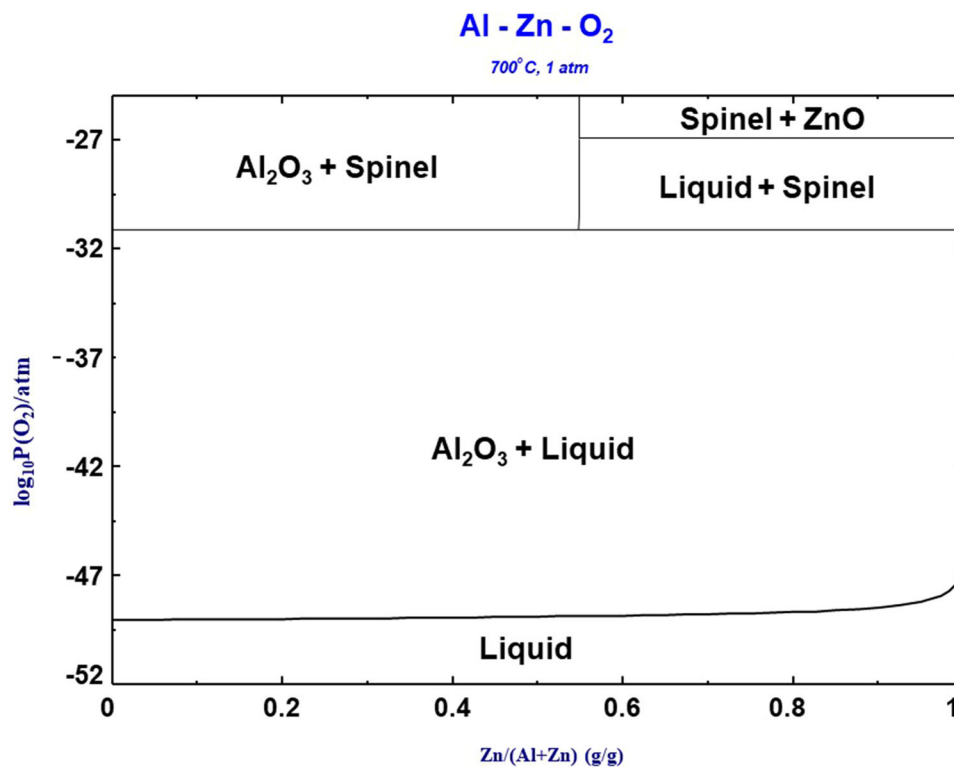

Figure 12. Phase diagram of Al–Zn system plotted for Zn mass fraction versus oxygen partial pressure at 700 °C calculated by FactSage 7.3.[32]
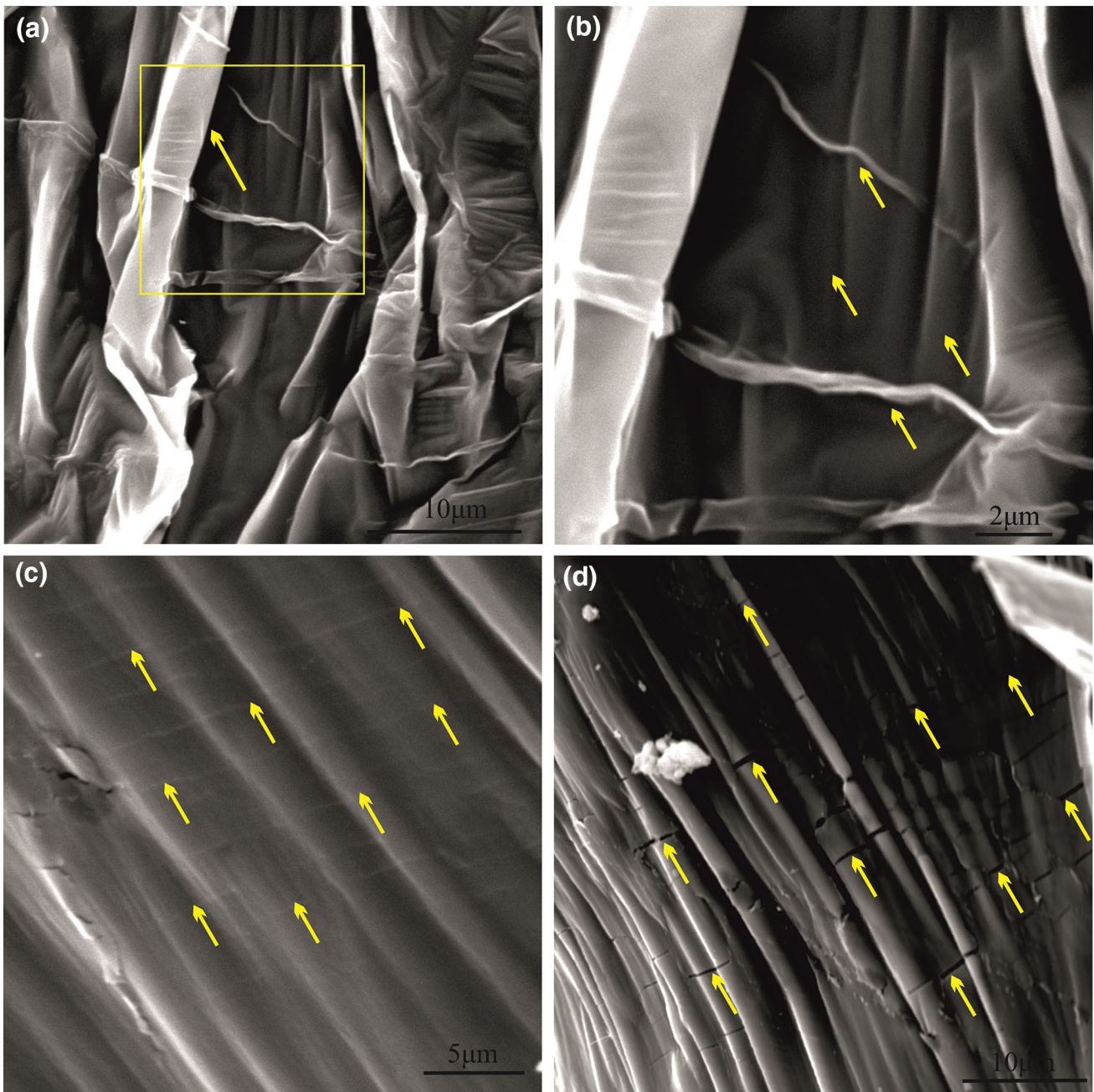
Figure 13. *SEM images of OMO sandwiches which show cracks and non-cracks on the surface of the oxide layers: (a) pure aluminum, (b) magnified area of (a) showing no sign of cracks, (c) Al–3%Zn and (d) Al–7%Zn. Note the reduced flexibility of the oxide film as a result of Zn addition.*

REFERENCES

1. E.N. Coker, The oxidation of aluminum at high temperature studied by thermogravimetric analysis and differential scanning calorimetry. Advanced Materials Laboratory, Sandia National Laboratories (2013). https://doi.org/10.2172/1096501
2. M. Drouzy, C. Mascré, Metall. Rev. **14**(1), 25–46 (1969)
3. S.J. Bonner, J.A. Taylor, J.Y. Yao, M.A. Rhamdhani, Oxidation of commercial purity aluminum melts: an experimental study, in *Light Metals, The Minerals,*

Metals and Materials Series, ed. by B.A. Sadler (2016), pp. 993–997

4. J.M. Park, Behaviors of biofilms in A356 alloy during solidification: developing observation techniques with 3D micro X-ray tomography. Ph.D. Dissertation, School of Metallurgy and Materials College of Engineering, The University of Birmingham, 2009

5. P.K. Yuen, Effects of strontium on the oxidation of molten aluminum alloys containing silicon and magnesium. Ph.D. Dissertation, McGill University, 2001

6. S.J. Bonner, A microstructural and kinetic study of molten aluminium oxidation in relation to dross formation. Ph.D. dissertation, School of Mechanical and Mining Engineering, The University of Queensland, 2015

7. G. Wightman, D.J. Fray, Metall. Trans. B **14**, 625–663 (1983)

8. J. Campbell, *Complete Casting Handbook Metal Casting Processes, Metallurgy, Techniques and Design* (Elsevier Butterworth-Heinemann, Oxford, 2015)

9. S.A. Azarmehr, M. Divandari, H. Arabi, Mater. Sci. Technol. **28**(11), 1295–1300 (2012)

10. J. Campbell, J. Mater. Sci. **51**(1), 96–106 (2015)

11. M. Divandari, J. Campbell, Trans. AFS **01–048**, 8–10 (2001)

12. J. Campbell, Int. Metalcast. **1**, 7–20 (2007). https://doi.org/10.1007/BF03355414

13. C. Vian, Int. Metalcast. **8**, 59–60 (2014). https://doi.org/10.1007/BF03355573

14. C. Lee, T. So, K. Shin, Inter. Metalcast. **13**, 880–889 (2019). https://doi.org/10.1007/s40962-019-00307-2

15. D. Dispinar, J. Campbell, Mater. Sci. Eng. A **528**(10), 3860–3865 (2011)

16. J. Campbell, Inter. Metalcast. **6**, 7–18 (2012). https://doi.org/10.1007/BF03355529

17. M. Divandari, J. Campbell, Alum. Trans. **2**(2), 233–238 (2000)

18. M. Divandari, Mechanisms of bubble damage in castings. Ph.D. dissertation, School of Metallurgy and Materials, The University of Birmingham, 2001

19. M. Divandari, J. Campbell, Int. J. Cast Met. Res. **17**(3), 182–187 (2004)

20. M. Divandari, M. Mehrabian, J. Mat. Sci. Eng. **14**(3), 34–47 (2017)

21. M.M. Jalilvand, N.T. Bagh, M. Akbarifar, A. Divandari, Int. Metalcast. (2019). https://doi.org/10.1007/s40962-019-00395-0

22. I. Haginoya, T. Fukusako, IMONO **54**, 664–669 (1982). https://doi.org/10.11279/imono.54.10-664

23. W. Kahl, E. Fromm, Metall. Mater. Trans. B **16**, 47–51 (1985)

24. J. Liu, Q. Wang, Y. Qi, Acta Mater. **164**, 673–682 (2019)

25. M. Divandari, J. Campbell, Int. J. Cast Metal Res. **18**(3), 16–21 (2005)

26. M.M. Jalilvand, M. Akbarifar, M. Divandari, H. Saghafian, J. Magnes, Alloy **8**(1), 219–230 (2020)

27. Y. Waseda, K.T. Jacob, T. Tsuchiya, S. Tamaki, J. Mater. Sci. Lett. **33**(8), 940–945 (1978)

28. M.G.C. Cox, B. Mcenaney, V.D. Scott, Nat. Phys. Sci. **237**, 140–142 (1972)

29. M.G.C. Cox, B. Mcenaney, V.D. Scott, Philos. Mag. **26**(4), 839–851 (1972)

30. X. Jhou, H. Habazaki, K. Shimizu, P. Skeldon, G.E. Thompson, G.C. Wood, Corros. Sci. **38**(9), 1563–1577 (1996)

31. E.M. Hinton, The oxidation of liquid aluminium and the potential for oxides in grain refinement of aluminium alloys. Ph.D. dissertation, University of Birmingham, 2014

32. C.W. Bale, E. Bélisle, P. Chartrand, Comput. Coupl. Phase Diagr. Thermochem. **54**, 35–53 (2016)

33. G.M. Scamans, E.P. Butler, Met. Trans. A **6**, 2055–2063 (1975)

34. M. Syvertsen, Oxide skin strength on molten AA5XXX aluminum alloy-effect of beryllium and alternatives, in *Light Metals*, (2017) pp. 1451–1455. https://doi.org/10.1007/978-3-319-0_173

35. S. Saha, C. Ravindran, Inter. Metalcast. **9**, 39–48 (2015). https://doi.org/10.1007/BF0335603